Journal of Statistical Mechanics: Theory and Experiment
An IOP and SISSA journal

PAPER: Classical statistical mechanics, equilibrium and non-equilibrium

Dynamics of granular particles with interactions at a distance

Raquel E Rojas-Martínez, Pedro Díaz-Leyva and Rodrigo Sánchez[1]

Departamento de Física, Universidad Autónoma Metropolitana Unidad Iztapalapa, Av. San Rafael Atlixco 186, Col. Vicentina C.P. 09340, Ciudad de México, Mexico
E-mail: rodrsanchez@xanum.uam.mx

Received 12 July 2019
Accepted for publication 25 October 2019
Published 10 January 2020

Online at stacks.iop.org/JSTAT/2020/013207
https://doi.org/10.1088/1742-5468/ab54b9

Abstract. A system of granular particles with interactions at a distance is studied experimentally, and the corresponding dynamics is examined via the speed distributions. It is found to differ from that of hard granular systems, i.e. systems with no interactions other than dissipative collisions, and the discrepancy is shown to not be due solely to the effect of interactions on clustering. Finally, analytical expressions are derived and compared to the experimental results.

Keywords: stationary states, cluster aggregation

J. Stat. Mech. (2020) 013207

[1] Author to whom correspondence should be addressed.

1742-5468/20/013207+15$33.00

Contents

1. Introduction

Granular particles dissipate kinetic energy during collisions and exhibit negligible Brownian motion [1–6], and their dynamics is thus inherently out of thermodynamic equilibrium if they are not at rest. Thus, even in the absence of interactions other than collisions, their speeds generally do not follow the Maxwell–Boltzmann distribution [1, 3, 5, 7], although there are exceptions [8, 9]. Dissipation favours clustering [4, 5], which is interrelated with the dynamics [3, 5, 10]; the latter can be studied via the speed distributions [3, 10].

The following 2D speed distribution, derived from a 1D speed distribution obtained for simulational granular systems [3], and that has been applied to the angular velocities of elongated externally driven particles [11], has been used for hard (i.e. interacting solely via collisions) granular systems [10–12]:

$$f_{2D}(v) = Cv \sum_{m=1}^{M} \exp\left(-\frac{(v/v_0)^2 m^\beta}{2}\right) \exp(-\alpha m), \tag{1}$$

where $f_{2D}(v)$ is the fraction of speeds (moduli of the 2D velocities) found between v and $v + \mathrm{d}v$, M is the total number of particles in the system, v_0 is a characteristic speed and C is a normalization constant. Particles are assumed to be in clusters of size m (with $m = 1$ corresponding to lone particles) having speed distributions of the same form as those of quasi-2D non-dissipative hard particles in thermal equilibrium, i.e. the 2D Maxwell–Boltzmann form, but with a peak at $v_0 m^{-\beta/2}$ (and therefore explicitly dependent on cluster size), where β is a dimensionless parameter, and on N_m, the number of particles in clusters of size m, being proportional to $\exp(-\alpha m)$ [3, 10], where α is also dimensionless. The 2D Maxwell–Boltzmann form is recovered in the limit $\beta \to 0$.

$f_{2D}(v)$ has been shown to apply to experimental granular systems of quasi-2D (defined as systems whose constituents cannot have the same 2D coordinates [4, 6,

J. Stat. Mech. (2020) 013207

13–15]) externally driven particles [10, 11] and binary mixtures [10], and to self-propelled particles [12]. Importantly, the 1D distribution from which it is derived is itself obtained from simulations explicitly considering viscous drag. Likewise, experimental validation of this distribution [11], and of the 2D distribution derived from it [10, 12], has been for systems in air, not in a vacuum, including gently agitated systems of light particles [12] for which air resistance is unlikely to be negligible.

The dynamics of granular systems with interactions other than collisions are not only of clear fundamental interest, but are also of practical interest. There is evidence, for example, that electrostatic repulsion due to triboelectric charge affects the dynamics [16]. Furthermore, all experimental systems are to some extent soft (deformable), and there is evidence that soft granular particles can be modelled using interaction potentials [17, 18]. The effect of external potentials on granular dynamics, the most ubiquitous of which is gravity, is perhaps even more important. A 3D granular speed distribution must, in all conditions save microgravity, consider gravitational potential energy, as must speed distributions of quasi-2D and quasi-1D systems that are not on a level plane.

The literature on interacting granular particles has typically focused on systems subject to gravity and with repulsive contact forces as the only interparticle interactions (such as the simulational work of Langston *et al* [19] or of Cleary and Sawley [20]). Typically net flows have been examined rather than speed distributions of individual particles [19]. Only very rarely have such distributions been examined for particles with interactions at a distance, such as in the work of Kohlstedt *et al* [21], which involves an external field inducing interparticle interactions.

In the present work, we examine the experimental speed distributions of a system of circular granular particles with directional interactions at a distance on an air/water interface. In order to ensure that interactions have a distinct effect on clustering without hindering it, directional interactions were chosen so that interaction energy is minimised by a Kagome lattice (see figure 1), of interest in its own right [22–25] but which has been studied to the best of our knowledge only in systems with non-dissipative collisions, including in the simulational literature. Dissipative collisions, in the absence of interactions at a distance, tend to favour dense, glass-like structures or close-packed lattices [4, 5, 17, 26].

2. Materials and methods

2.1. Particles and cell

Circular, token-like (diameter $\sigma = 29$ mm and 5 mm thickness) particles were made via 3D printing (poly(lactic acid) FDM20 3D printer, Proyectil) using an infill of 15 % to help ensure flotation. Each particle has two pairs of diametrically opposite slits (3 mm $\times$ 1.5 mm $\times$ 2 mm each) on the top side, with the diameters joining each pair at 60° from each other, in an X-shaped arrangement, as shown in figure 2. Neodymium magnets (1 mm height, 2 mm diameter, N50 from HuoXing Appliance & Lighting Store) were glued in place in the slits with alternating poles facing outwards. Particle centres were marked with white paint to assist identification. Finished particles have a 2.19 g mass.

J. Stat. Mech. (2020) 013207

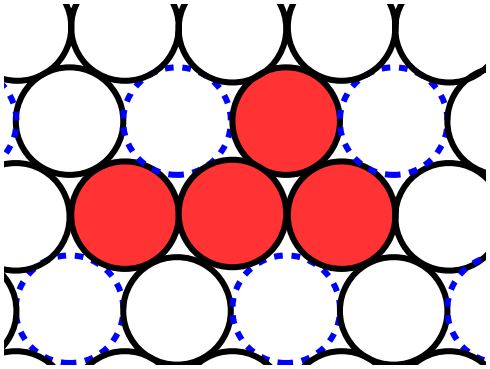

Figure 1. The lattices relevant to our system are shown schematically. If all circles are considered, they form a close-packed lattice. The solid circles (black) form a Kagome lattice. The filled circles (red) constitute a small cluster compatible with both close-packed and Kagome lattices.

For the magnets used, interactions become negligible beyond ∼3 mm face-to-face distance. Their effective range, their interactions' directionality and the particles' dimensions ensure that a magnet on a given particle can only have a non-negligible interaction with one other magnet at a time and that these interactions become important only at an edge-to-edge distance that is small on the scale of particle diameter. Capillary interactions are much weaker than magnetic interactions.

A 45.3 cm × 45.3 cm × 4.5 cm acrylic cell, painted black, was filled with 2000 ml of water and two opposing corners were then placed on inflated rubber bladders, in turn on two speakers (200 W subwoofers); the bladders maximize transmission of mechanical energy from the speakers to the cell and minimize loss as noise (see figure 2). Placing the speakers underneath the cell ensures there is no direct interaction between them and the particles, as the water lies between them. The speakers themselves are driven by a sinusoidal wave with a frequency of 4.5 Hz (Hewlett Packard 3314A signal generator and 500 W Kinter WA-150 amplifier). This frequency corresponds to the empirically determined full system's resonant frequency, as determined by the water surface's vibration's amplitude, and therefore minimizes overall power loss. The cell's characteristic dimensionless acceleration Γ ($= A\omega^2/g$, where A is the water surface's vibration's amplitude, ω is the driving angular frequency and g is the acceleration due to gravity) is ∼0.4. No flipping motion, nor any instances of multilayers, were observed during the experiments, confirming the system remains quasi-2D. Much larger amplitudes would likely lead to fully 3D behaviour, and much lower Γ would lead to a system entirely dominated by bonding.

After the onset of agitation, and in order to ensure reproducible initial conditions, a grid (square lattice) was placed at the centre of the cell, and the number of particles used for any given experiment were placed in the grid, forming a rectangle with no vacancies at the grid's centre. The grid was then lifted vertically out of the water, and the system is then allowed to evolve freely. $t = 0$ in the analysis corresponds to the first frame captured without the grid.

Particle numbers were chosen on the basis of being high enough to ensure good statistics, but low enough to allow significant time evolution in the system.

J. Stat. Mech. (2020) 013207

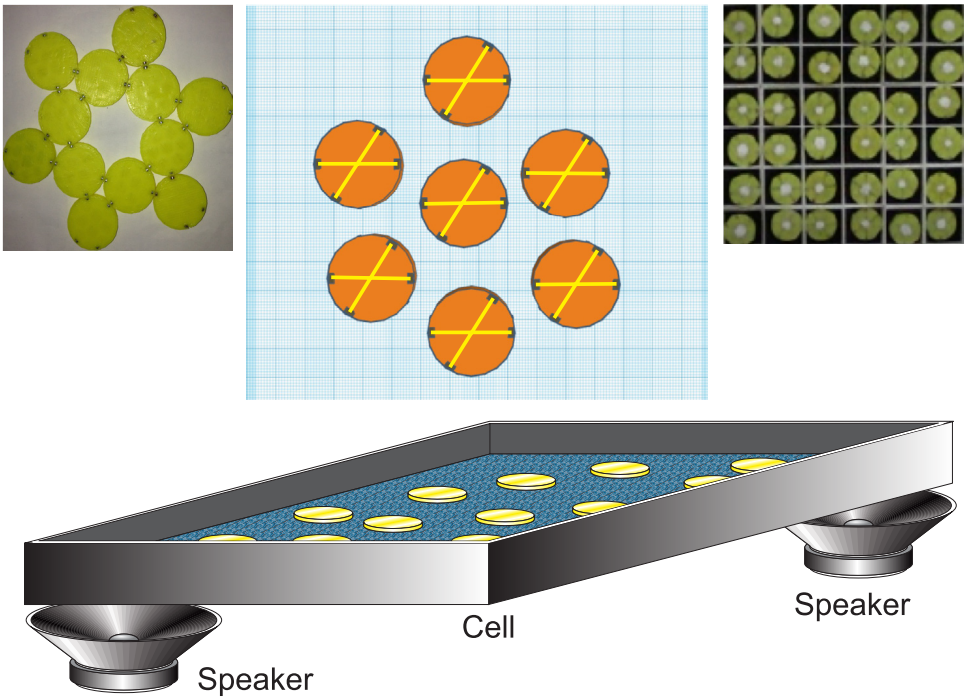

Figure 2. The experimental set-up is shown schematically (bottom). Two speakers under opposite corners of the cell drive the cell to oscillate along the vertical direction; the remaining corners are on fixed custom-made supports (not shown) with rubber spheres to ensure bouncing and thus minimise loss of kinetic energy; these supports also minimize lateral motion. The central inset shows the design used for 3D printing of the particles used; slits for the magnets are in an X-shaped arrangement, as depicted by the overlaid crosses. The top left inset shows a segment of a Kagome lattice held together by magnetic attractions between particles with magnets prior to marking their centres. The remaining inset (top right) shows the central region of a 144 particles experiment's initial conditions.

2.2. Forces and interactions

There are only two forces in our system that are absent in experimental systems whose distributions have been successfully described by $f_{2D}(v)$ [10–12], and that are also not considered in the simulations of Puglisi *et al* [3]: magnetic interactions and capillary interactions arising from the particles being at an interface. Capillary forces between particles at an interface and moving along it can be modelled as interparticle interactions at a distance with an attractive potential proportional to r^{-4} [27, 28]; as magnetic and capillary interactions are independent phenomena, the net interaction is simply the sum of the magnetic and capillary interactions. This situation is distinct from that studied by Buck *et al* [29], in which granular particles move perpendicularly to the surface of a liquid, whereas in our experiments the particles remain at the air/water interface and move along it. Two particles placed in contact with each other such that equal magnetic poles are facing each other move apart immediately, showing that magnetic interactions are much stronger than capillary forces. While capillary forces alone would introduce interactions at a distance, the addition of stronger magnetic interactions ensures interactions at a distance wholly dominate the behaviour, as is

J. Stat. Mech. (2020) 013207

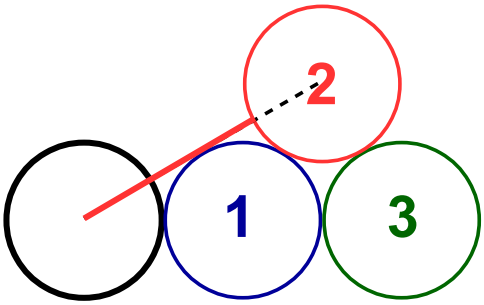

Figure 3. A cluster compatible with both Kagome and close-packed lattices (see figure 1) is shown. The particles labelled '1' (blue), '2' (red) and '3' (green) are first, second and third-nearest neighbours, respectively, of the black particle on the left. Nearest neighbours are a distance $r = \sigma$ away; for second-nearest neighbours $r = \sqrt{3}\sigma \approx 1.7321\sigma$ (solid (red) and dashed lines combined) [26, 31–33] and for third-nearest neighbours $r = 2\sigma$. Thus the shell of second-nearest neighbours' inner edge is at $r = (\sqrt{3} - 1/2)\sigma \approx 1.2321\sigma$, depicted by the solid (red) line; the shell of third-nearest neighbours' inner edge is at $r = 1.5\sigma$. Using a cut-off of $r = (\sqrt{3} - 1/2)\sigma$ ensures the inclusion of nearest neighbours while excluding second-nearest neighbours.

desirable since their effect, and how the resulting dynamics differs from that in non-interacting systems, is the focus of the present work. Capillary attractions favour dense clusters, as does dissipation.

Aside from these interactions at a distance, our system is fundamentally similar to that reported by Cadillo–Martínez and Sánchez [10], for which single particles and small clusters are prevalent.

2.3. Image capture and analysis

Videos were captured at a rate of 29 frames per second by a Canon VIXIA HF R70 (1920 $\times$ 1080 pixels) camera placed above the cell centre. Taking a particle length divided by the root mean squared speed of a particle, for the time segments used to obtain speed distributions, a characteristic time $\approx$6 s is obtained, beyond which a particle could not be reliably distinguished from a neighbour based on two images captures at such an interval, i.e. beyond which trajectories cannot be reliable tracked. This characteristic time is long enough for over 100 frames to be captured, i.e. the time between frames is two orders of magnitude smaller. Thus the frame rate used is adequate for tracking particles and measuring speeds in these systems.

Trajectories were obtained by enhancing the images using ImageJ and tracking the particles using the plug-in Mosaic [30]. Further analysis was carried out using software written in-house.

2.4. Clustering, speed distributions and statistics

Two particles are identified as being in the same cluster if their centres are under $(\sqrt{3} - 1/2)\sigma$ apart (see figure 3).

Various functions are compared with speed histograms normalised by the number of data points used to produce them, i.e. with fractional frequencies. From probabilistic

J. Stat. Mech. (2020) 013207

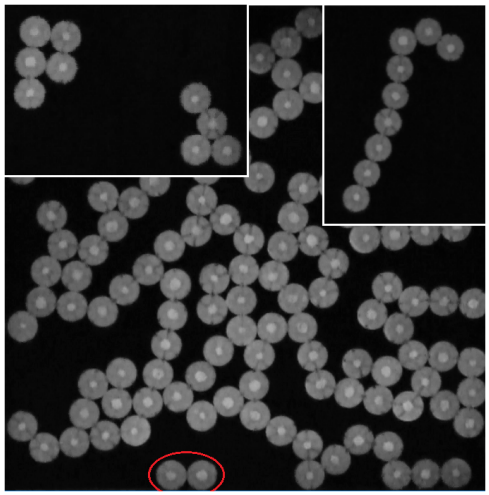

Figure 4. The main picture shows the last frame from an experiment with 144 particles. A dimer separate from the main cluster is highlighted by a red ellipse. The insets show the last frame for two separate experiments with nine particles.

considerations, the theoretical uncertainty of the normalised histograms shown is of $\sqrt{\nu(1-\nu)/N_T}$, where ν is the fractional frequency and N_T is the total number of data points used for the histogram. Two types of systems are examined in greater detail (90 and 144 particles). For 90 particles (the system with poorer statistics of the two), and since 500 frames are used for the intervals shown, $N_T \sim 4.5 \times 10^4 \cdot \nu$ in practice remains below ∼0.1, and thus this uncertainty has a maximum value of ∼0.001, i.e. about 1% of the peak value. A similar analysis for histograms using longer time intervals for systems with 9 particles yields a maximum uncertainty of ∼2% of the peak value. These histograms therefore have sufficiently good statistics to provide physically meaningful insights, while the time intervals used are brief enough to preclude significant time-dependence in the histograms, as our focus is on behaviour once rapid changes from the initial conditions have taken place and not on the system's long-term evolution.

3. Results and discussion

As illustrated by the examples shown in figure 4, the experiments reach a steady state in which all or nearly all the particles have joined a single cluster, made up mainly of slightly arched rows, segments arranged in a Kagome formation and, particularly for the highest particle concentration, a few segments reminiscent of a close-packed crystal. This can be understood as the result of competition between interactions, which favour the formation of a single Kagome crystal, and dissipation and capillary attractions, which favour the formation of a dense cluster; the densest possible configuration is a close-packed crystal. Rows are compatible with both a Kagome and a close-packed crystal (see figure 3), and slightly arched rows lead to a more compact cluster than purely straight ones. These rows resemble the structures formed by simulational disks with four interaction sites at low packing fractions, which at higher packing fractions form

J. Stat. Mech. (2020) 013207

Kagome crystals [24], despite differences in the nature of the interactions involved, and in the angles between the interaction sites.

The system's behaviour is thus dominated neither by interactions nor by dissipation, but rather results from competition between them. This scenario is not only likely to arise in practice in many granular systems with interaction potentials, but is also of particular fundamental interest since the extremes -negligible potential energy, and systems governed entirely by potentials- can be understood as limiting cases of competition between dissipation and potentials.

The systems with nine particles result in different final configurations, typically consisting of either a single cluster (such as the one shown in the top right-hand corner of figure 4) or of two clusters (such as the ones shown in the top left-hand corner of figure 4); the larger systems typically have a main, stable cluster containing most, in some frames all, of the particles in the system and few (especially for the systems with 144 particles) medium-sized clusters (in the example shown in the main picture in figure 4, there is a large main cluster, and a dimer can be seen next to the bottom edge of the picture, but no medium-sized clusters are found). Beyond these qualitative similarities, cluster size distributions vary substantially between individual experiments (data not shown) and do not collapse onto a single form, especially for systems with 90 particles, which is unsurprising given that granular systems often exhibit non-linear dynamics [34–36] and chaotic behaviour [34, 35]. The system being highly sensitive to even minute variations in initial conditions, as is usual in systems with non-linear dynamics, likely accounts for the variations between speed distributions of similarly prepared individual experiments, which are comparable to those of other experimental systems [10].

As shown in figure 5, after ≈20 s the systems reach a stationary state and, except for the large fluctuations for one of the 9 particles systems, are remarkably similar. Thus for further analysis, we focus on the two larger system sizes (90 and 144 particles) and on the behaviour in the last 500 frames of each experiment, unless indicated otherwise.

As shown in figure 6, $f_{2D}(v)$, which describes the behaviour of hard granular particles, can be reasonably fitted to the experimental data at low speeds (below about 0.1 σs^{-1}), but not at high ones. The leading order term in the series expansion is linear in v for both the 2D Maxwell–Boltzmann distribution and for $f_{2D}(v)$, and the fitted β values are very small (typically in the 10^{-5}–10^{-3} range) compared to those reported for other systems [3, 10–12]. More importantly, the fitted values of both α and β are within theoretical uncertainties of zero. Therefore, according to our results $f_{2D}(v)$ is not significantly better than the 2D Maxwell–Boltzmann distribution, and it fits the data well at low speeds.

This can be understood in terms of energetics; at low speeds, kinetic energies are feeble compared to the binding energies due to magnetic attractions, and therefore these particles can be plausibly assumed to move as a rigid body. Therefore, collisions between slow particles are infrequent, as they would require them to first separate from their neighbours. For the systems with 144 particles, the clusters' centre of mass speeds in the same intervals as the data used for figure 6 are ∼0.06 σs^{-1} (data not shown), which is well within the regime in which the speed distribution is well-described by $f_{2D}(v)$. Thus in this regime particle speeds are predominantly related to overall cluster motion, which is consistent with bonds neither forming nor breaking. If, as in other

J. Stat. Mech. (2020) 013207

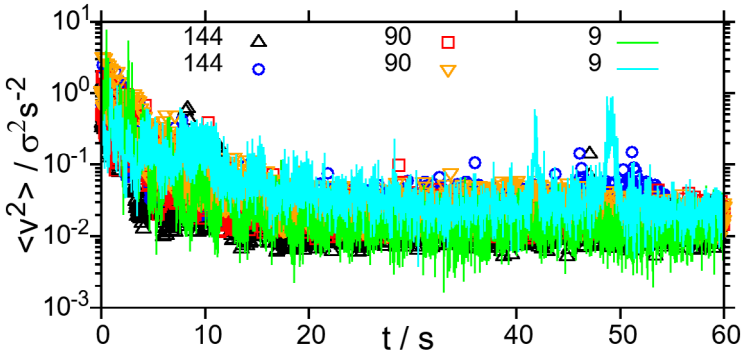

Figure 5. Mean squared speeds are shown as functions of time for the first minute of six independent experiments. The key indicates the number of particles in each experiment. Mean squared speeds decrease and then fluctuate around a stable value, and despite order-of-magnitude differences in the number of particles the results are quantitatively comparable. After ≈20 s (final 40 s in the figure) mean squared speeds fluctuate but do not evolve in any discernible pattern, suggesting any long-term ageing takes place over times ≫40 s. Since the mean squared speed is proportional to the mean kinetic energy, this can be taken as a reasonable indicator that a stationary or metastable state has been reached. Since the data analysed for the speed distributions of the larger systems is taken over ≈17 s, these distribution correspond to 'snapshot' of the system's dynamics unaffected by long-term ageing.

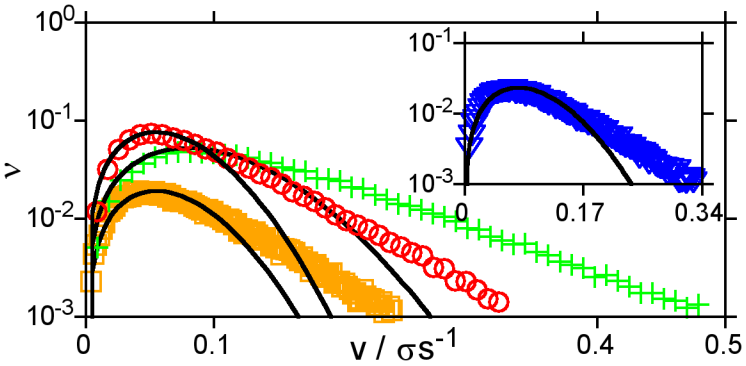

Figure 6. The main figure shows the experimental speed distributions (symbols) for three independent experiments with 144 particles, as well as least squares fits to $f_{2D}(v)$. The fitted parameters (see main text) are, with v_0 in units of σs^{-1}: $v_0 = 0.103 \pm 8.6$, $\alpha = -0.0985 \pm 7.79 \times 10^8$ and $\beta = 4.8210^{-6} \pm 6505$ for +'s (green), $v_0 = 0.0642 \pm 82.8$, $\alpha = -0.0985 \pm 7.90 \times 10^8$ and $\beta = 1.88 \times 10^{-4} \pm 2.54 \times 10^4$ for empty circles (red), and $v_0 = 0.0589 \pm 69.2$, $\alpha = -0.0994 \pm 9.26 \times 10^8$ and $\beta = 1.69 \times 10^{-4} \pm 2.63 \times 10^4$ for empty squares (orange). The inset likewise shows the data and fitted $f_{2D}(v)$ for an experiment with 90 particles ($v_0 = 0.0771 \pm 2.09$, $\alpha = -0.102 \pm 1.26 \times 10^9$ and $\beta = 1.13 \times 10^{-5} \pm 4641$).

granular systems [5, 37–39], slow-moving particles are mostly not at the clusters' edges, as is plausible given that they would have more neighbours to bind with, then neither do they directly collide with free particles. Their dynamics is therefore governed by Brownian-like agitation and by viscous drag, i.e. it is qualitatively similar to that of thermal systems.

On the other hand, the high kinetic energies corresponding to high speeds could, despite dissipation and despite interactions, break apart or structurally modify existing clusters, so the role of interactions becomes crucial. There are essentially two ways in which interactions can affect the speed distributions. They may affect cluster formation and breaking, and therefore the factor of $\exp(-\alpha m)$ in $f_{2\mathrm{D}}(v)$ may no longer hold. Separately, they may modify the dynamics separately from their effect on clustering. We first examine the former effect.

If interparticle interactions affect the speed distribution solely via the clustering, then the following speed distribution would be obeyed:

$$f_{2\mathrm{D}}^{(1)}(v) = Cv \sum_{m=1}^{M} N_m \exp\left(-\frac{(v/v_0)^2 m^\beta}{2}\right), \tag{2}$$

where N_m is the experimentally measured number of particles in clusters of size m in the particular data set to be fitted, which eliminates one adjustable parameter, and the remaining parameters have the same physical interpretation as before. Since N_m is explicitly included, there is in principle no need to restrict analysis to stationary states or brief time intervals, since even if clustering is evolving, that will be included in the N_m values, and system agitation and other mechanical properties are kept constant. Experimentally, particles are overwhelmingly found in large clusters (of size $\approx M$) and a much smaller number is found in small clusters, while virtually no medium-sized clusters are observed, which can be understood in terms of binding energies. Once a large cluster forms, small clusters or single particles breaking off require only a few bonds to break, so the energetic cost is low, but a medium-sized cluster breaking off would generally require breaking a larger number of bonds and is thus energetically less favourable.

Figure 7 shows that $f_{2\mathrm{D}}^{(1)}(v)$ fits the data well at modest speeds, but fails at large speeds. This shows that interactions have an effect on the dynamics beyond affecting clustering, and that this is greater for high kinetic energies. Since the first term of the series expansion of $f_{2\mathrm{D}}^{(1)}(v)$, of $f_{2\mathrm{D}}(v)$ and of the 2D Maxwell–Boltzmann distribution are all of the same form (a linear term), it is unsurprising that $f_{2\mathrm{D}}^{(1)}(v)$ fits the data well at modest speeds. The fact that systems with few particles are better described overall by $f_{2\mathrm{D}}^{(1)}(v)$ than larger ones hints at collective effects being important in the high speeds regime.

In order to obtain a better analytical model for our data, we focus on the extremes of low and high speeds. As discussed earlier, slow particles likely have dynamics qualitatively similar to that of thermal systems, so we therefore assume:

$$f_{\mathrm{low}}(v) \approx C' v \exp\left(-\frac{1}{2}\left(\frac{v}{v_0'}\right)^2\right), \tag{3}$$

where $f_{\mathrm{low}}(v)$ is the speed distribution for low speeds and v_0' is analogous to v_0.

We now turn to the regime of high speeds. We assume that the fastest-moving particles have escaped, either individually or in small clusters, from the main cluster's edge. We furthermore assume that, right before escaping, they were relatively fast-moving and loosely bound. Since more free particles mean more gaps and fewer bonds at the main cluster's edge, we assume the probability of release is proportional to the

J. Stat. Mech. (2020) 013207

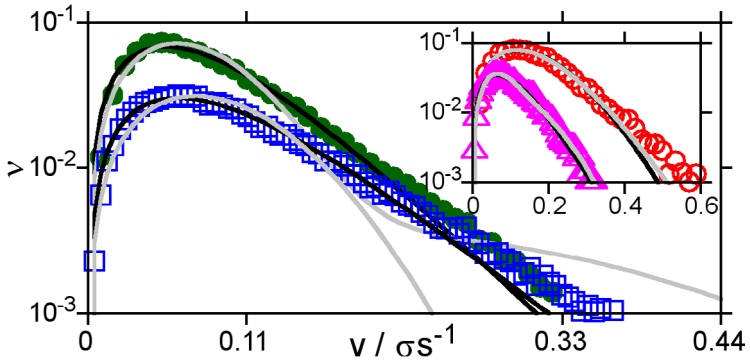

Figure 7. Speed distributions of the final 500 frames of two independent experiments with 144 particles (main figure) and of all but the first 300 frames (eliminating any transients from the onset of the experiment) of two experiments with nine particles (inset) are shown. Gray lines correspond to least squares fits to $f_{2D}^{(1)}(v)$ and black lines to least squares fits to $g_{2D}(v)$ (see text). For the data sets in the main figure, the fitted parameters are (see main text), with v_0 and v_0' in units of σs^{-1} and γ in units of $s\sigma^{-1}$: $v_0 = 0.254 \pm 0.0137$, $\beta = 0.573 \pm 0.0221$, $v_0' = 0.637 \pm 0.591$ and $\gamma = 23.7 \pm 0.422$ for filled circles (dark green) and $v_0 = 0.0786 \pm 0.560$, $\beta = 0.0194 \pm 2.87$, $v_0' = 318 \pm 3.75 \times 10^7$ and $\gamma = 20.5 \pm 0.251$ for empty squares (blue). For the inset, the fitted parameters are: $v_0 = 0.238 \pm 0.006\,00$, $\beta = 0.980 \pm 0.0455$, $v_0' = 0.175 \pm 0.007\,54$ and $\gamma = 6.71 \pm 0.507$ for empty circles (red), and $v_0 = 0.159 \pm 0.001\,94$, $\beta = 1.04 \pm 0.0197$, $v_0' = 0.253 \pm 0.0350$ and $\gamma = 18.7 \pm 0.459$ for empty triangles (magenta).

number of particles that are already free. Therefore, the number of particles in this regime that are released after travelling a distance $\mathrm{d}x$ is given by:

$$\mathrm{d}N_{\mathrm{rel}} = P(\text{release between } x \text{ and } x + \mathrm{d}x)N_{\mathrm{rel}}, \tag{4}$$

where P(release between x and $x + \mathrm{d}x$) is the probability, per particle that is already free, of a loosely bound particle being released after travelling a distance $\mathrm{d}x$, and x is the particle position. If we assume particles are released at random places along the main cluster's edge, then we can write:

$$P(\text{release between } x \text{ and } x + \mathrm{d}x) = \eta \mathrm{d}x, \tag{5}$$

where η is a positional density of events that release a particle. Therefore:

$$\mathrm{d}N_{\mathrm{rel}} = \eta N_{\mathrm{rel}} \mathrm{d}x. \tag{6}$$

Loose particles at the main cluster's edge must move, between collisions and other interactions, comparatively rapidly, even if they do so more slowly than fully free particles. Plausibly, they move rapidly enough that the net force acting on them is predominantly viscous drag, and thus:

$$F_{\mathrm{net}}(v_{\mathrm{loose}}) \approx -\xi v_{\mathrm{loose}}, \tag{7}$$

where $F_{\mathrm{net}}(v_{\mathrm{loose}})$ is the net force and ξ is the drag coefficient. Note that $\langle F_{\mathrm{net}}(v_{\mathrm{loose}})\rangle = -\xi \langle v_{\mathrm{loose}}\rangle$, since the agitation force fluctuates around zero. In this regime, the speed decays exponentially and the speed and displacement differentials can therefore be related by:

$$\mathrm{d}x = -\frac{\mathrm{d}v_{\mathrm{loose}}}{\xi}. \tag{8}$$

Putting this together with our earlier result for $\mathrm{d}N_{\mathrm{rel}}$, we obtain:

$$\mathrm{d}N_{\mathrm{rel}} = -\frac{\eta N_{\mathrm{rel}}}{\xi}\mathrm{d}v_{\mathrm{loose}}. \tag{9}$$

Rearranging and integrating, this yields, if most of the time η varies slowly with N_{rel} (for sufficiently high N_{rel} it must become negative, as otherwise the main cluster would break down completely, but we assume at modest N_{rel} η varies little):

$$N_{\mathrm{rel}} = N_i \exp\left(-\frac{\eta v_{\mathrm{loose}}}{\xi}\right), \tag{10}$$

where N_i is an integration constant. This equation governs the relationship between the number of free particles and their speed immediately before being released. If the relationship between v_{loose} and the actual speeds of the particles once they become free is at least approximately linear, then we have:

$$N_{\mathrm{rel}}(v) \sim N_i' \exp\left(-\gamma v\right), \tag{11}$$

where γ is a constant and N_i' is a normalization constant. Once particles with a certain value of v_{loose} are free, their speeds will vary due to agitation forces and viscous drag. By assumption, as these are free particles collisions will be much less frequent than for loosely bound particles. Thus we expect deviation from the above equation to be governed by a distribution of the 2D Maxwell–Boltzmann form. We can combine both this behaviour and the behaviour of N_{rel} as follows:

$$f_{\mathrm{high}}(v) \approx C' v \exp\left(-\frac{1}{2}\left(\frac{v}{v_0'}\right)^2\right) \exp\left(-\gamma v\right), \tag{12}$$

where C' is a normalization constant and v_0' is analogous to v_0 in $f_{\mathrm{2D}}(v)$.

We therefore seek a function that tends to $f_{\mathrm{low}}(v)$ at low speeds and to $f_{\mathrm{high}}(v)$ at high speeds, not only as matter of convenience but, more fundamentally, also because the regimes we have considered are not necessarily unambiguously distinct; for instance, the boundary between tightly bound particles deep within the main cluster and loosely bound particles near the edge might not be sharply defined.

Inspired by Padé approximants [40, 41], we postulate a speed distribution of the following form:

$$g_{\mathrm{2D}}(v) = \frac{C' f_{\mathrm{num}}(v)}{1 + f_{\mathrm{den}}(v)}, \tag{13}$$

and since both $f_{\mathrm{low}}(v)$ and $f_{\mathrm{high}}(v)$ involve a factor of $v\exp\left(-\frac{1}{2}\left(v/v_0'\right)^2\right)$, we set $f_{\mathrm{num}}(v) = v\exp\left(-\frac{1}{2}\left(v/v_0'\right)^2\right)$. $g_{\mathrm{2D}}(v)$ then tends to $f_{\mathrm{low}}(v)$ at low speeds, provided $f_{\mathrm{den}}(v)$ tends to a constant greater than -1 in this limit. For $g_{\mathrm{2D}}(v)$ to tend to $f_{\mathrm{high}}(v)$ at high speeds, $(1 + f_{\mathrm{den}}(v))^{-1}$ must tend to $\exp\left(-\gamma v\right)$. These requirements are satisfied by $f_{\mathrm{den}}(v) = \exp\left(\gamma v\right)$, yielding:

J. Stat. Mech. (2020) 013207

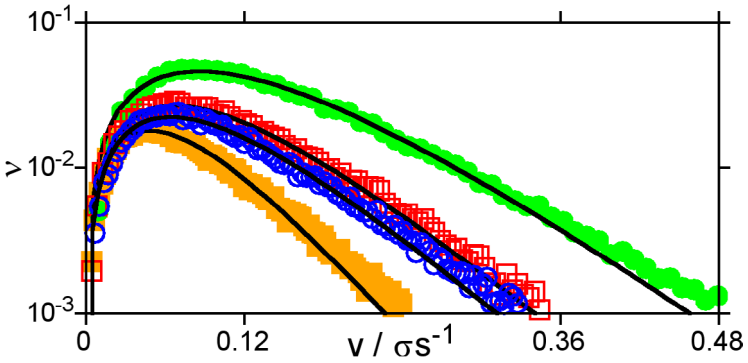

Figure 8. Speed distributions are shown for two independent experiments with 144 particles (filled symbols) and for two independent experiments with 90 particles (empty symbols). Lines correspond to least squares fits to $g_{2D}(v)$. The experiments with 144 particles are separate experiments from those whose data is shown in figure 7. The fitted parameters are, in units of σs^{-1} and of $s\sigma^{-1}$: $v_0' = 0.541 \pm 0.106$ and $\gamma = 14.5 \pm 0.194$ for filled circles (green), $v_0' = 573 \pm 1.91 \times 10^8$ and $\gamma = 18.9 \pm 0.237$ for empty squares (red), $v_0' = 2.83 \pm 31.8$ and $\gamma = 19.9 \pm 0.31$ for empty circles (blue), and $v_0' = 302 \pm 5.19 \times 10^7$ and $\gamma = 26.2 \pm 0.317$ for filled squares (orange).

$$g_{2D}(v) = \frac{C' v \exp\left(-\frac{1}{2}(v/v_0')^2\right)}{1 + \exp\left(\gamma v\right)}. \tag{14}$$

This has the same number of adjustable parameters as $f_{2D}^{(1)}(v)$. The low and high speeds regimes correspond to $v \ll \gamma^{-1}$ and to $v \gg \gamma^{-1}$, respectively, and the thermodynamic equilibrium form is recovered in the limit $\gamma \to 0$.

As shown in figures 7 and 8, $g_{2D}(v)$ fits the data well for both large and small systems, and while there is a modest discrepancy at large speeds, it is much smaller than those of $f_{2D}(v)$ or $f_{2D}^{(1)}(v)$ for large systems. In addition, it requires no explicit knowledge of cluster sizes or even of the total number of particles in the system. This is an important advantage since, especially for systems in which the number of particles examined is not fixed or is not known *a priori*, determining the values of N_m for each individual experiment may be impractical, and the computational cost of fitting either $f_{2D}(v)$ or $f_{2D}^{(1)}(v)$ increases rapidly with the number of particles.

$f_{2D}(v)$ has been shown to describe the speed distributions of spheres, permanent dimers of spheres [10], egg-shaped particles [11] and particles with straight edges [12]; $f_{2D}(v)$ has been shown to be applicable to a wide variety of hard granular systems. The derivation of $g_{2D}(v)$ makes no assumptions regarding particle geometry nor that of the interactions, so it is not unreasonable to propose that it may likewise be applicable to a wide range of interacting granular systems. At a minimum, it is likely to be applicable to related geometries with similar interactions, such as particles with interaction sites at other angles. Future work will focus on exploring the consequences of varying the interactions involved, including varying their geometry. This research may shed light on the physical aspects governing γ or, alternatively, on the relationship between the nature of the interactions and the type of functions that can accurately describe the speed distribution. It should be noted that the data of Kohlstedt *et al* [21], involving

J. Stat. Mech. (2020) 013207

both an external field and interparticle interactions appears to be qualitatively of the same form as our distributions, and it is possible it could be well-described by $g_{2D}(v)$.

4. Conclusions

Experimental granular submonolayers with magnetic interactions were used to examine granular dynamics in the presence of strong interparticle interactions. The formation of a large, low density, main cluster is consistently observed. The particles' speed distributions differ from those of hard granular particles and we analytically model the low and high speed limits separately.

Speed distributions in the system examined have been successfully described for a variety of particle numbers by an analytic expression combining physical models of the behaviour at high and low speeds. Future work will focus on extending these results to other granular systems with interactions.

Acknowledgments

The authors acknowledge financial support from Conacyt (Fronteras de la Ciencia 2015-02-1450) and technical assistance from A Muñoz–Franco and from E S Santos–Rivera, as well as valuable discussions with G A Chapela.

References

[1] Goldhirsch I and Zanetti G 1993 Clustering instability in dissipative gases *Phys. Rev. Lett.* **70** 1619–22
[2] Iverson R M 1997 The physics of debris flows *Rev. Geophys.* **35** 245–96
[3] Puglisi A, Loreto V, Marini Bettolo Marconi U, Petri A and Vulpiani A 1998 Clustering and non-Gaussian behavior in granular matter *Phys. Rev. Lett.* **81** 3848–51
[4] Olafsen J S and Urbach J S 1998 Clustering, order, and collapse in a driven granular monolayer *Phys. Rev. Lett.* **81** 4369–72
[5] Tobochnik J 1999 Granular collapse as a percolation transition *Phys. Rev.* E **60** 7137
[6] Aronson I S and Tsimring L S 2006 Patterns and collective behavior in granular media: theoretical concepts *Rev. Mod. Phys.* **78** 641–92
[7] Puglisi A, Gnoli A, Gradenigo G, Sarracino A and Villamaina D 2012 Structure factors in granular experiments with homogeneous fluidization *J. Chem. Phys.* **136** 014704
[8] Costantini G, Marconi U M B, Kalibaeva G and Ciccotti G 2005 The inelastic hard dimer gas: a nonspherical model for granular matter *J. Chem. Phys.* **122** 164505
[9] Tapia-Ignacio C, Garcia-Serrano J and Donado F 2016 Nonvibrating granular model for a glass-forming liquid: equilibration and aging *Phys. Rev.* E **94** 062902
[10] Cadillo-Martínez A T and Sánchez R 2017 Experimental velocity distributions in a granular submonolayer *Physica* A **465** 221–8
[11] Sánchez R and Díaz-Leyva P 2018 Rotational and translational dynamics of anisotropic granular particles *J. Stat. Mech.* 083210
[12] Sánchez R and Díaz-Leyva P 2018 Self-assembly and speed distributions of active granular particles *Physica* A **499** 11–9
[13] Santana-Solano J and Arauz-Lara J L 2001 Hydrodynamic interactions in quasi-two-dimensional colloidal suspensions *Phys. Rev. Lett.* **87** 038302
[14] Blair D L and Kudrolli A 2003 Collision statistics of driven granular materials *Phys. Rev.* E **67** 041301
[15] Reis P M, Ingale R A and Shattuck M D 2007 Caging dynamics in a granular fluid *Phys. Rev. Lett.* **98** 188301

[16] Sánchez R, Huerta A and Aguirre-Manzo L A 2016 Dynamics and orientational order of a charged granular fluid *Granular Matter* **18** 1–7
[17] Burton J C, Lu P Y and Nagel S R 2013 Collision dynamics of particle clusters in a two-dimensional granular gas *Phys. Rev.* E **88** 062204
[18] Sánchez R and Morales-Martínez C L 2016 Cluster evolution in a soft granular submonolayer *J. Stat. Mech.* 123203
[19] Langston P A, Tüzün U and Heyes D M 1995 Discrete element simulation of granular flow in 2D and 3D hoppers: dependence of discharge rate and wall stress on particle interactions *Chem. Eng. Sci.* **50** 967–87
[20] Cleary P W and Sawley M L 2002 DEM modelling of industrial granular flows: 3D case studies and the effect of particle shape on hopper discharge *Appl. Math. Modelling* **26** 89–111
[21] Kohlstedt K, Snezhko A, Sapozhnikov M V, Aranson I S, Olafsen J S and Ben-Naim E 2005 Velocity distributions of granular gases with drag and with long-range interactions *Phys. Rev. Lett.* **95** 068001
[22] Syôzi I 1951 Statistics of kagomé lattice *Prog. Theor. Phys.* **VI** 306–8
[23] Chen Q, Bae S C and Granick S 2011 Directed self-assembly of a colloidal kagome lattice *Nature* **469** 381–4
[24] Chapela G A, Guzmán O, Martínez-González J A, Díaz-Leyva P and Quintana H J 2014 Self-assembly of kagome lattices, entangled webs and linear fibers with vibrating patchy particles in two dimensions *Soft Matter* **10** 9167–76
[25] Fejer S N and Wales D J 2015 Design of a Kagome lattice from soft anisotropic particles *Soft Matter* **11** 6663–8
[26] Sánchez R, Romero-Sánchez I C, Santos-Toledano S and Huerta A 2014 Polydispersity and structure: a qualitative comparison between simulations and granular systems data *Rev. Mex. Fis.* **60** 136–41
[27] Stamou D and Duschl C 2000 Long-range attraction between colloidal spheres at the air-water interface: the consequence of an irregular meniscus *Phys. Rev.* E **62** 5263–72
[28] Danov K D, Kralchevsky P A, Naydenov B N and Brenn G 2005 Interactions between particles with an undulated contact line at a fluid interface: capillary multipoles of arbitrary order *J. Colloid Interface Sci.* **287** 121–34
[29] Buck B, Lunewski J, Tand Y, Deen N G, Kuipers J A M and Heinrich S 2018 Numerical investigation of collision dynamics of wet particles via force balance *Chem. Eng. Res. Des.* **132** 1143–59
[30] Sbalzarini I F and Koumoutsakos P 2005 Feature point tracking and trajectory analysis for video imaging in cell biology *J. Struct. Biol.* **151** 182–95
[31] Tobochnik J and Chapin P M 1988 Monte Carlo simulation of hard spheres near random closest packing using spherical boundary conditions *J. Chem. Phys.* **88** 5824–9
[32] Lubachevsky B D, Stillinger F H and Pinson E N 1991 Disks versus spheres: contrasting properties of random packings *J. Stat. Phys.* **64** 501–24
[33] Truskett T M, Torquato S, Sastry S, Debenedetti P G and Stillinger F H 1998 Structural precursor to freezing in the hard-disk and hard-sphere systems *Phys. Rev.* E **58** 3083–8
[34] Hill K M, Khakhar D V, Gilchrist J F, McCarthy J J and Ottino J M 1999 Segregation-driven organization in chaotic granular flows *Proc. Natl Acad. Sci.* **96** 11701–6
[35] Banigan E J, Illich M K, Stace-Naughton D J and Egolf D A 2013 The chaotic dynamics of jamming *Nat. Phys.* **9** 288–92
[36] Liu L, Li J and Wan C 2018 Nonlinear dynamics of excited plate immersed in granular matter *Nonlinear Dyn.* **91** 147–56
[37] Paolotti D, Cattuto C, Marini Bettolo Marconi U and Puglisi A 2003 Dynamical properties of vibrofluidized granular mixtures *Granular Matter* **5** 75–83
[38] Sánchez R and Huerta A 2015 Dynamics and avalanches in a system exhibiting granular collapse *Physica* A **437** 367–74
[39] Wang Z and Zhang J 2015 Spatiotemporal chaotic unjamming and jamming in granular avalanches *Sci. Rep.* **5** 8128
[40] Baker G A and Graves-Morris P 1996 *Padé Approximants* (Cambridge: Cambridge University Press)
[41] Sader J E 1997 Accurate analytic formulae for the far field effective potential and surface charge density of a uniformly charged sphere *J. Colloid Interf. Sci.* **188** 508–10

J. Stat. Mech. (2020) 013207